JGR Oceans

RESEARCH ARTICLE
10.1029/2019JC016017

Seasonal Variation of the Deep Limb of the Pacific Meridional Overturning Circulation at Yap-Mariana Junction

Jianing Wang[1,2,3], Qiang Ma[1], Fan Wang[1,2,3], Youyu Lu[4], and Larry J. Pratt[5]

[1]Key Laboratory of Ocean Circulation and Waves, Institute of Oceanology, Center for Ocean Mega-Science, Chinese Academy of Sciences, Qingdao, China, [2]Laboratory for Ocean and Climate Dynamics, Qingdao National Laboratory for Marine Science and Technology, Qingdao, China, [3]University of Chinese Academy of Sciences, Beijing, China, [4]Fisheries and Oceans Canada, Bedford Institute of Oceanography, Dartmouth, Nova Scotia, Canada, [5]Woods Hole Oceanographic Institution, Woods Hole, MA, USA

Abstract This study reveals the seasonal variability of the lower and upper deep branches of the Pacific Meridional Overturning Circulation (L-PMOC and U-PMOC) in the Yap-Mariana Junction (YMJ) channel, a major gateway for deep flow into the western Pacific. On the western side of the YMJ channel, mooring observations in 2017 and in 1997 show the seasonal phase of the L-PMOC at depths of 3,800–4,400 m: strong northward flow with speed exceeding 20 cm s^{-1} and lasting from December to next May and weak flow during the following 6 months. On the eastern side of the channel, mooring observations during 2014–2017 show two southward deep flows with broadly seasonal phases, one being the return flow of L-PMOC below ~4,000 m and with the same phase of L-PMOC but reduced magnitude. The second, shallower, southward deep flow corresponds to the U-PMOC observed within 3,000–3,800 m and with opposite phase of L-PMOC, that is, strong (weak) southward flow appearing during June–November (December–May). Seasonal variations of the L-PMOC and U-PMOC are accompanied by the seasonal intrusions of the Lower and Upper Circumpolar Waters (LCPW and UCPW) in lower and upper deep layers, which change the isopycnal structure and the deep currents in a way consistent with geostrophic balance.

Plain Language Summary The role of the deep Pacific Ocean in regulating the global climate is influenced by the Pacific Meridional Overturning Circulation (PMOC). The general pathways of the lower and upper branches of the deep part of the PMOC (L-PMOC and U-PMOC) have been sketched out, but their detailed temporal variations remain unclear. In the Yap-Mariana Junction, a major chokepoint for L-PMOC and U-PMOC flowing into the western Pacific, mooring observations were made in 2017 and in 1997 on the western side of the channel and were conducted during 2014–2017 on the eastern side of the channel. Analysis on the observed currents reveals broadly seasonal variations of the L-PMOC and U-PMOC with the opposite phase. The L-PMOC flows northward at depths below ~3,800 m during December–May on the western side of the channel and is accompanied by a weaker southward return flow on the eastern side. The U-PMOC flows southward at depths over ~3,000–3,800 m during June–November on the eastern side. Further analysis of numerical ocean modeling results demonstrates that the seasonal and spatial variations of the L-PMOC and U-PMOC are related to the intrusions of the Lower and Upper Circumpolar Waters.

Key Points:
- Lower and upper branches of PMOC (L-PMOC and U-PMOC) show broadly seasonal variation with opposite phase in Yap-Mariana Junction channel
- L-PMOC flows northward during December–May on western side of channel, and U-PMOC flows southward during June–November on eastern side
- Seasonalities of L-PMOC and U-PMOC are related to geostrophically balanced seasonal intrusions of Lower and Upper Circumpolar Waters

Correspondence to:
F. Wang,
fwang@qdio.ac.cn

Citation:
Wang, J., Ma, Q., Wang, F., Lu, Y., & Pratt, L. J. (2020). Seasonal variation of the deep limb of the Pacific meridional overturning circulation at Yap-Mariana junction. *Journal of Geophysical Research: Oceans*, *125*, e2019JC016017. https://doi.org/10.1029/2019JC016017

Received 24 DEC 2019
Accepted 21 MAY 2020
Accepted article online 27 MAY 2020

1. Introduction

The North Pacific is an immense reservoir for heat and carbon, with long residence times, making it an important component of the global climate system (Johnson et al., 2007). Due to the lack of local formation, the deep and bottom waters of the North Pacific Ocean have their origins in the Antarctic and are carried by the northward deep part of the Pacific Meridional Overturning Circulation (PMOC), much of which is contained in the Pacific Deep Western Boundary Current. However, the deep limb of the PMOC is not as well observed as the lowest limb of the Atlantic Meridional Overturning Circulation.

Based on previous mooring and hydrography measurements, the deep limb of the PMOC is partitioned into the lower and upper branches (L-PMOC and U-PMOC), located in the lower and upper deep layers, respectively (Kawabe et al., 2006, 2009; Kawabe & Fujio, 2010). North of the midlatitude in the south Pacific, the two layers correspond to potential temperature $\Theta < 1.2$°C at depths greater than ~3,500 m and 1.2–2.2°C at

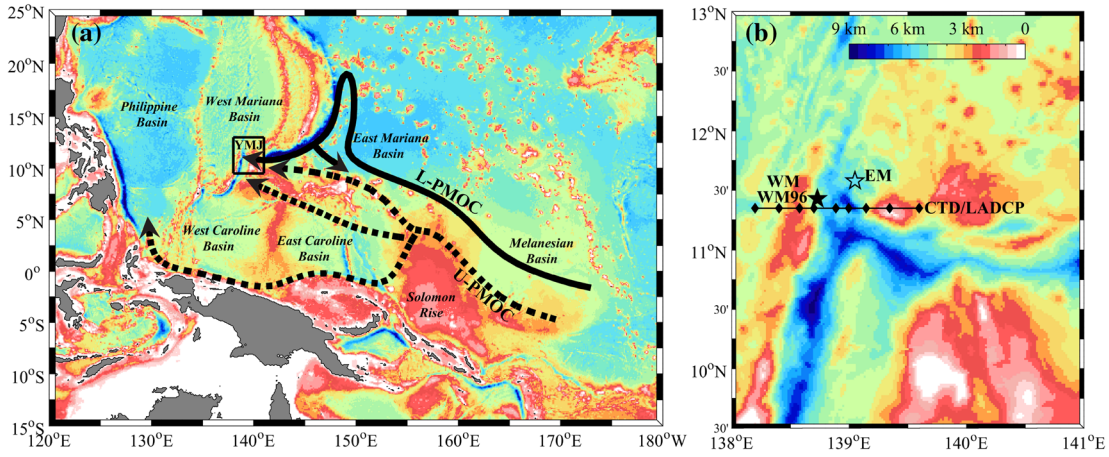

Figure 1. (a) Bathymetry (color shading) of the Western Pacific Ocean and schematic pathways of L-PMOC and U-PMOC (solid and dashed arrows, based on Kawabe & Fujio, 2010). The black rectangle in panel a shows (b) the bathymetry of the Yap-Mariana Junction (YMJ). Locations of mooring sites on the western (WM96 and WM, solid pentagram) and eastern (EM, blank pentagram) sides of the YMJ channel and CTD/LADCP stations along 11.35°N (diamonds) are marked in panel b.

depths of ~2,000–3,500 m, respectively (Kawabe et al., 2006, 2009). Both L-PMOC and U-PMOC are separated from the Antarctic Circumpolar Current. The L-PMOC flows northward to the east of New Zealand and then to the east of the Tonga-Kermadec Ridge (Whitworth et al., 1999). After passing through the Samoan Passage (Rudnick, 1997; Voet et al., 2015) or around the Manihiki Plateau (Pratt et al., 2019), it enters the Central Pacific Basin and bifurcates into the eastern and western branches (Johnson & Toole, 1993; Kawabe et al., 2003, 2006). The western branch passes through the Melanesian and East Mariana Basins and finally flows into the western Pacific through the deep channel at the Yap-Mariana Junction (YMJ; solid black arrow in Figure 1a, Huang et al., 2018; Kawabe & Fujio, 2010; Siedler et al., 2004). The U-PMOC flows northward in the South Pacific, detouring around the subtropical gyres (Reid, 1997) and entering the equatorial Pacific after passing east of Solomon Rise (Kawabe et al., 2006; Kawabe & Fujio, 2010). It then flows into the Philippine Sea by way of the East and West Caroline Basins and partly via the East Mariana Basin (Kawabe et al., 2003) through the YMJ channel (dashed black arrow in Figure 1a). The L-PMOC and U-PMOC carry the Lower and Upper Circumpolar Waters (LCPW and UCPW), respectively. Both LCPW and UCPW have their origin in the Southern Ocean (Callahan, 1972; Mantyla & Reid, 1983). As the remnant of North Atlantic Deep Water, the LCPW is characterized by a salinity maximum and a silica minimum (Johnson & Toole, 1993). In comparison with LCPW, UCPW is relatively warm, fresh, oxygen-poor, and silica-rich (Kawabe et al., 2006; Kawabe & Fujio, 2010). The potential temperature $\Theta = 1.2°C$ is often used as the boundary to separate the LCPW and UCPW (e.g., Johnson et al., 1994; Johnson & Toole, 1993).

In the deep channel of the YMJ, the L-PMOC carries the LCPW with potential temperature (Θ) less than 1.2°C and at depths below ~4,000 m (Siedler et al., 2004). Through upwelling and mixing, LCPW can be transformed into the North Pacific Deep Water (NPDW; Kawabe & Fujio, 2010), a process accompanied by a loss of dissolved oxygen (DO). The NPDW is mainly formed in the northeastern Pacific but can be transported westward to the East Mariana Basin in a layer with Θ of 1.2–2.2°C and at depths of ~2000–4,000 m (Kawabe & Fujio, 2010; Siedler et al., 2004). The UCPW carried by the U-PMOC occupies almost the same depth range of the NPDW. Compared to the NPDW, the UCPW is characterized by slightly higher DO and salinity (S); however, the boundary between the NPDW and UCPW is difficult to identify locally (Kawabe & Fujio, 2010).

At the YMJ, the flow characteristics in the deep channel were first revealed by observations with moored current meters deployed on the western side of the channel from October 1996 to March 1998 (hereafter referred to as WM96; as reported by Siedler et al., 2004). At depths below 3,200 m, the record of four current meters showed that the deep flow was directed northward in alignment with the channel direction and with a 16-month averaged speed reaching a maximum of 10.4 cm s^{-1} at 4,220 m. Joint analyses with hydrographic observations suggested that the deep and bottom layers were dominated by NPDW and LCPW, respectively.

At 3,220 and 4,220 m, the northward flow speed increased (decreased) in time as the water temperature decreased (increased). Although Siedler et al. (2004) presented the data from their moorings, they did not discuss seasonal variability.

Factors that motivated the present work include a desire to better understand seasonal changes in the deep flow at the YMJ and to investigate the possibility that strong currents might exist on the eastern side of the channel. It is also recognized that the YMJ is an important choke point (Siedler et al., 2004) and therefore an advantageous site for long-term monitoring the climatologically important deep limb of the PMOC. With these issues in mind we deployed new moorings and conducted hydrography surveys in the YMJ channel beginning in 2014 (Figure 1b). These moorings are a part of the Scientific Observing Network of the Chinese Academy of Sciences (CASSON) in the western Pacific. The rest of the paper is organized as follows. Section 2 introduces the data used in this study. Section 3 describes temporal-spatial variations of the observed PMOC in the YMJ channel. Section 4 elucidates the dynamic processes of temporal-spatial variations of the PMOC with the aid of model outputs and climatological data. Discussion and conclusions are present in Section 5.

2. Data

2.1. Mooring Data

Two subsurface moorings were recently deployed on the western and eastern sides of the deep channel at YMJ, referred to as WM and EM, respectively (Figure 1b). The distance between WM and EM is approximately 80 km. The WM was deployed at 138.7°E, 11.4°N on 22 November 2016, and recovered on 4 December 2017. The EM was first deployed at 139.0°E, 11.6°N on 14 August 2014, redeployed twice on 9 November 2015 and 18 November 2016 for maintenance, and finally recovered on 3 December 2017. The water depths of the WM and EM sites are ~4,726 and ~5,200 m, respectively. The WM was equipped with one upward-looking 75 kHz Teledyne RD Instruments (TRDI) acoustic Doppler current profiler (ADCP) at ~500 m and several discrete JFE INFINITY-Deep current meters and SBE 37-SM conductivity-temperature-depths (CTDs) below that. The EM was equipped with one upward- and one downward-looking 75 kHz TRDI ADCPs at ~500 m and several discrete Nortek Aquadopp current meters, SBE 56 and RBR temperature loggers (Ts), and SBE 37-SM CTDs below that. The ADCPs hourly measured the upper ocean velocity over the depth ranges of 50–500 m at the WM site and 50–1,050 m at the EM site with a bin size of 8 m, and the data were then interpolated vertically to standard depths. Current meters returned hourly records of point velocity in the deep layers. Ts measured temperature every 10 minutes. CTDs sampled temperature, salinity, and pressure every 10 minutes. Note that the dissolved oxygen sensors were equipped on EM SBE 37-SM CTDs at several deep depths from 9 November 2015 to 17 November 2016 and sampled the data every 10 minutes as well. All data were first low-pass filtered with a 72-h Lanczos filter to remove the effects of inertial fluctuations and tides and then averaged to derive the daily means.

Two decades ago, one subsurface mooring (WM96) was deployed at 138.7°E, 11.4°N on 13 October 1996, and recovered on 8 March 1998 (Figure 1b; Siedler et al., 2004). WM and WM96 occupied almost the same location. The water depth of WM96 is 4,720 m. Four Aanderaa current meters measured velocity and temperature at 3,220, 3,720, 4,220, and 4,670 m. The two-hourly recorded data were also low-pass filtered and then averaged to obtain the daily means.

2.2. CTD/LADCP Section

During the cruise to maintain the moorings EM and WM in 2016, shipboard measurements of water properties (including salinity, temperature, and pressure) and velocity profiles were made with an SBE 911plus CTD and a set of two TRDI lowered ADCPs (LADCP) attached to the water sample rosette. A section with nine CTD/LADCP stations was conducted across the YMJ channel along 11.35°N between 138.2°E and 139.6°E during 21–22 November 2016 (Figure 1b). On 8 March 1998 when WM96 was recovered, one CTD profile was also conducted at the WM96 site to obtain salinity, temperature, and pressure data (Siedler et al., 2004). These CTD data were post-processed to account for time lags between the temperature and conductivity sensor, for the thermal mass of the conductivity sensor, and to remove pressure inversions due to ship rolling before averaging to 1-m bins. Both the upward- and downward-looking LADCPs are operated at 300 kHz and 10-m bin size. The LADCP profiles were processed using an inversion method based on LDEO software (Visbeck, 2002). Velocity profiles were collected using 1 ping per ensemble with ensemble

sampled at 1 Hz during downcast and upcast and were then constrained using bottom-tracking velocity, ship drift data from GPS, and upper-ocean velocities measured by a 38 kHz shipboard ADCP.

2.3. Model Outputs

To investigate the underlying dynamics of temporal-spatial variations of the PMOC at the YMJ channel, we use daily fields of temperature, salinity, and velocity over 2013–2015 from a global ocean reanalysis product (GLORYS12V1) and over 2016–2018 from analysis product (PSY4V3R1), both created by Mercator Ocean (http://www.mercator-ocean.fr/). Outputs from these two products are merged into a single continuous time series (referred to as MO). The two products have the same nominal horizontal resolution of 1/12° in longitude/latitude and the same 50 vertical levels with a resolution of 1 m at the surface and of 450 m near the bottom, but the two are different in terms of assimilation of observation data. For more details on the two products, readers are referred to Lellouche et al. (2013, 2018).

2.4. AVISO Data

AVISO (Archiving, Validation, and Interpretation of Satellite Oceanographic) gridded sea level anomaly (SLA) and surface geostrophic current data with a resolution of 1/4° in longitude/latitude are used to study the influence of the upper ocean eddies on the deep currents. The eddy detection and tracking procedures used in this study are given by Chaigneau et al. (2008). Daily fields during observation periods are analyzed.

2.5. GDEM Data

The U.S. Navy Generalized Digital Environment Model (GDEM-V3.0) provides monthly climatology of temperature and salinity with a resolution of 1/4° in longitude/latitude. It has 78 vertical levels from the surface to 6,600 m, with a resolution varying from 2 m at the surface to 200 m below 1,600 m. The GDEM-V3.0 climatology for each month was derived from the Mater Oceanographic Observations Data Set by correcting the "erroneous" thermal inversions, where denser water overlies lighter water. In comparison with the world ocean atlas (WOA), GDEM-V3.0 improves the representation of salinity and density structure in the deep ocean (Carnes, 2009; Wang et al., 2011). The GDEM data are used to give the horizontal distribution of the potential density in the West and East Mariana Basins.

3. Observed PMOC

Figure 2 presents the time series of the daily-mean currents from the moorings WM and EM during their overlapping periods from 25 November 2016 to 2 December 2017. For the WM, the full-depth observations reveal a three-layered flow structure (red vectors in Figure 2): an upper layer dominated by zonal flow, including the westward North Equatorial Current (Figure 2a) and the eastward North Equatorial Undercurrent (Figure 2b); an intermediate layer between ~1,600 and 2,700 m with the significantly reduced flow speed (Figures 2c–2e); and the deep layer below 3,000 m with a nearly steady northward flow orientation but a significant temporal variability in magnitude (Figures 2f–2h). At 80 km to the east of the WM, the EM observations also capture a three-layered flow structure (blue vectors in Figure 2). In the upper layer, the flow speed and direction are both consistent with that at the WM site (Figures 2a and 2b). In the intermediate layer, the flow has a similar speed but with direction that is occasionally inconsistent with that at the WM site (Figures 2c–2e). In the deep layer, the flow speed is weaker, and the flow direction is mainly opposite to that at the WM site (Figures 2f–2h).

On the western side of the YMJ channel, a prominent seasonal variation of the deep flow can be revealed from two separate observations: the recent one in 2017 (WM) and the one 20 years ago in 1997 (WM96, Siedler et al., 2004). In the recent record, the intensified northward flow with speed reaching 20 cm s^{-1} at ~3,800 m persisted over 6 months from December 2016 to May 2017 but then diminished and experienced a north-south-oriented oscillation over the subsequent 6 months (red vectors in Figure 2). Similarly, the 1997 record shows that strong northward flow with speed reaching up to 45 cm s^{-1} at 4,220 m dominated the 6 months from December 1996 to May 1997 and was followed by a weak and more oscillatory phase lasting 6 months from June to November 1997 (Figure 3). In addition, the strong northward phase reappeared from December 1997 and lasted unitl the end of the measurements in March 1998. The strong and weak phases occurred during the same months, despite the fact that two records are separated by 20 years.

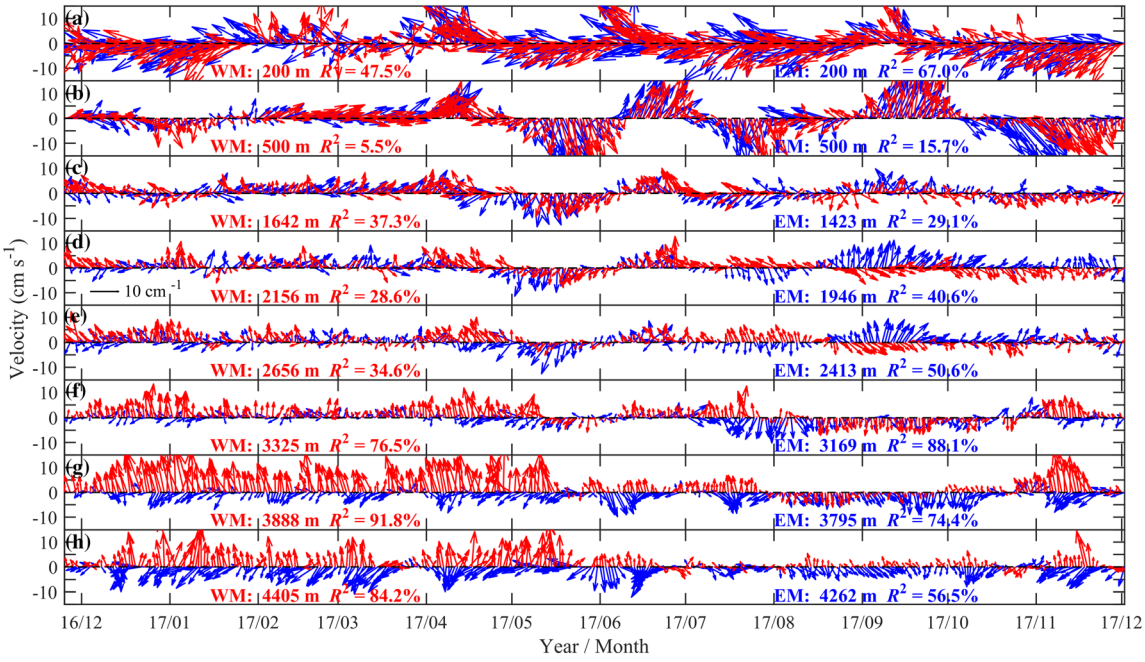

Figure 2. Stick plots of observed daily currents by WM (red) and EM (blue) spanning the upper, intermediate, and deep layers from 25 November 2016 to 2 December 2017. The numbers in red (blue) denote the mean depth of each velocity record during the whole measurement period and explained variance (R^2) for the annual harmonic of 91-day running mean meridional velocity from December 2016 to November 2017 from the WM (EM). A vector in upward direction corresponds to a northward flow. Tick-marks on the *x*-axis indicate the first day of each month (hereinafter the same).

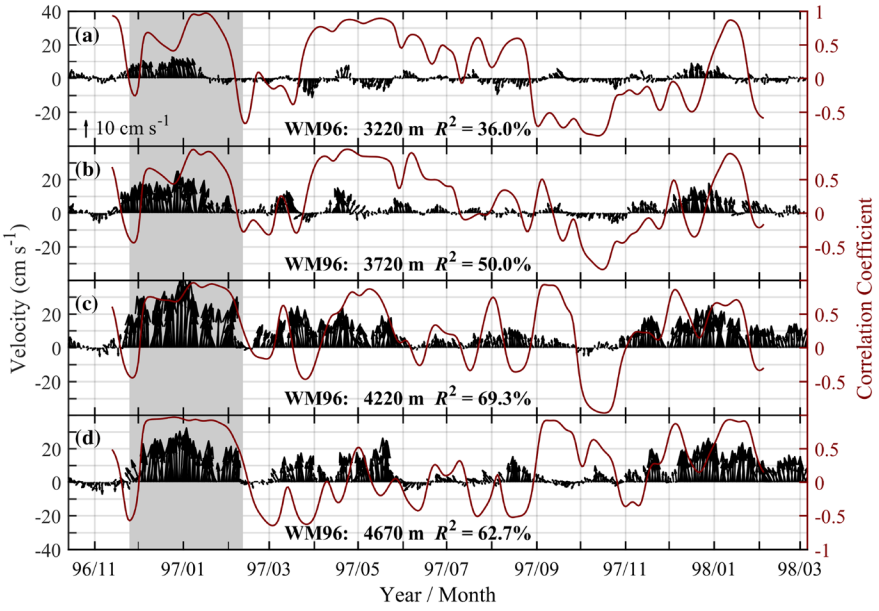

Figure 3. Stick plots of observed daily deep currents by WM96 at four depths from 14 October 1996 to 6 March 1998. The numbers in black denote the mean depth of each velocity record during the whole measurement period and explained variance (R^2) for the annual harmonic of 91-day running mean meridional velocity from December 1996 to November 1997. A vector in upward direction corresponds to a northward flow. Red curves show correlation coefficients (r) between the meridional components of observed deep flow and AVISO surface geostrophic current, calculated for 2-month segments sliding with time. Gray shading denotes the period when upper ocean eddies exerted influence on deep flow.

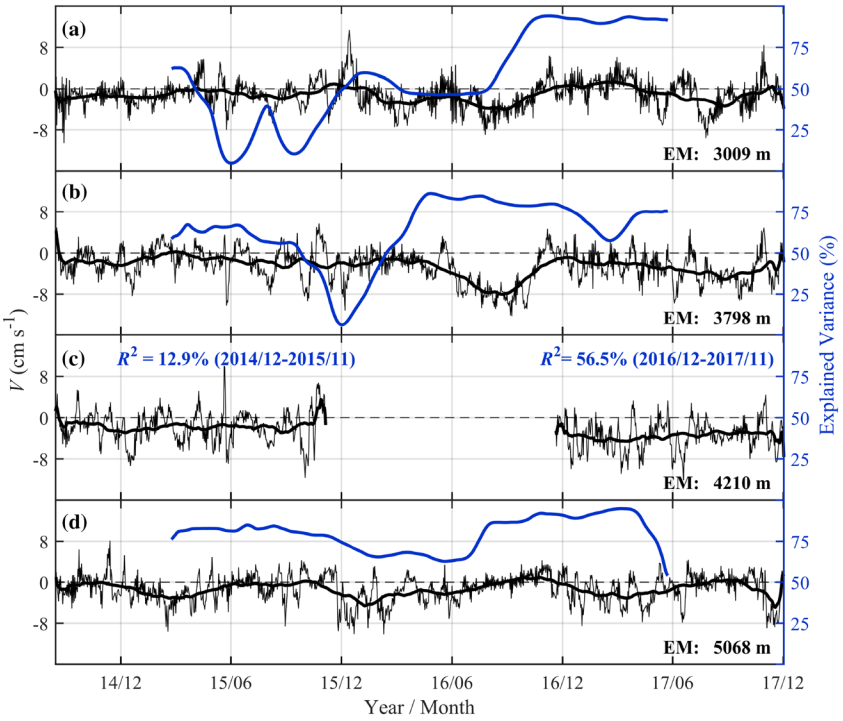

Figure 4. Time series of observed daily (thin) and 91-day running-mean (thick) deep meridional velocities by EM at four depths (numbers denoting mean depth of each record) from 14 August 2014 to 3 December 2017. In panels a, b, and d, blue curves show explained variance (R^2) for the annual harmonic of 91-day running mean meridional velocity, calculated for 365-day segments sliding with time. In panel c, the R^2 for the annual harmonic of 91-day running mean meridional velocity at 4,210 m from December 2014 to November 2015 and from December 2016 to November 2017 are denoted.

We also did an annual harmonic fit on the observed meridional velocity during December 2016–November 2017 and during December 1996–November 1997. Prior to the harmonic fit, the observed time series was smoothed by applying a 91-day running mean to focus on the variations longer than intraseasonal time scales. We calculated the explained variance (R^2), defined as a ratio of the variance of the fitted time series to the variance of the smoothed observations. On the western side of the channel, the R^2 values reach 76.5–91.8% for the deep meridional currents at depths of 3,225–4,405 m in the 2016–2017 record (Figure 2) and 50.0–69.3% at depths of 3,720–4,670 m in the 1996–1997 record (Figure 3).

On the eastern side of the YMJ channel, the structure of the deep meridional flow is more complicated. Accoring to the 2016–2017 record (Figure 2), the seasonal variation is strong at 3,169 m and 3,795 m depths, but the phases at both levels are opposite to that of northward deep flow on the western side; that is, on the eastern side the strong southward flow appearing over 6 months from June to November and weak flow during the following 6 months. The R^2 values for the two depths are 88.1% and 74.4%, respectively. We further extend the analysis to the whole 3-year long record during 2014–2017 (black curves in Figure 4). Consistent with the 2016–2017 record, the meridional velocity is mainly southward. After applying a 91-day running mean and then the annual harmonic fit, we calculate the R^2 values with overlapping 365-day segments and plot its time variation (blue curves in Figure 4). For the southward flows at 3,009 and 3,798 m depths, the explained variance of the seasonal cycle maintained a low value before 2016 and increased to more than 50% afterward. At 4,210 m, the seasonal cycle of southward flow is not obvious with very small R^2 of 12.9% before 2016 and become evident with R^2 of 56.5% in 2017. For the southward flow at 5,068 m, there is a strong seasonal variation with R^2 higher than 65% over nearly the whole measurement period. Furthermore, the seasonal phase of southward flows at 4,210 m during 2016–2017 and at 5,068 m during the whole measurement period is generally similar to that of the northward flow on the western side. The southward flow below ~4,200 m at the EM site appears to be the return of the northward flow at the WM site. During their strong phase from December 2016 to May 2017, the southward flow speed at 4,262 m of

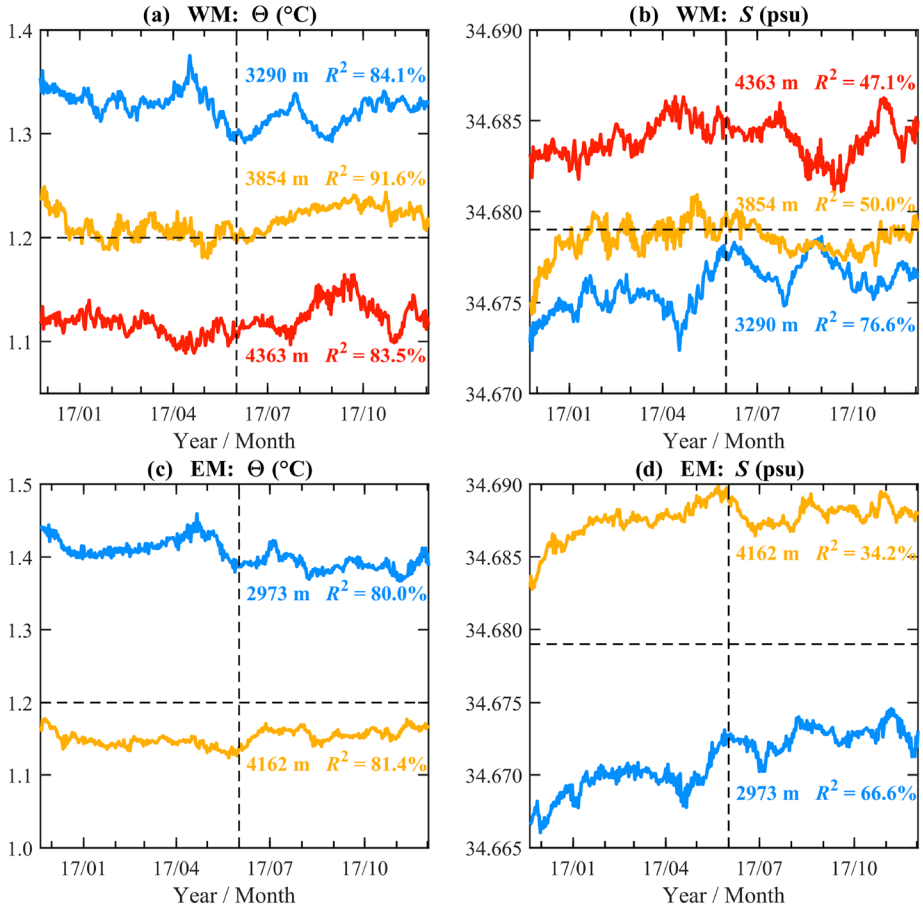

Figure 5. Time series of observed daily potential temperature (Θ, left) and salinity (*S*, right) by (a and b) WM from 24 November 2016 to 3 December 2017 and by (c and d) EM from 20 November 2016 to 2 December 2017. The numbers denote the mean depth of each velocity record during the whole measurement period and explained variance (R^2) for the annual harmonic of 91-day running mean Θ or *S* from December 2016 to November 2017. Dashed lines are used as reference lines to separate two seasonal phases and two watermasses (UCPW and LCPW, see text).

EM site is reduced by 36% compared to the northward flow speed at 4,405 m of WM site. We calculate their lead-lag correlation after applying a 41-day running mean to the observed time series. The correlation reaches a peak value of −0.45 at the 80% confidence level when WM leads EM by 37 days (figure not shown).

Variations of the deep flow on the western side of the YMJ channel were accompanied by changes in watermass properties. For the recent record, a decrease in deep layer Θ corresponded to an increase in *S* at the same depth and vice versa (Figures 5a and 5b). After applying a 91-day running mean and then the annual harmonic fit, we also calculate R^2 values for Θ and *S* at 3,290, 3,854, and 4,363 m depths during December 2016–November 2017. The seasonal cycles of watermass properties are strong with R^2 for Θ reaching 83.5–91.6% and R^2 for *S* reaching 47.1–76.6%. At 3,854 m, the time-averaged Θ and *S* were 1.21°C and 34.679 psu, very close to the upper boundary values (Θ = 1.2°C, *S* = 34.679) of the LCPW (e.g., Johnson et al., 1994; Johnson & Toole, 1993). Hence, the variation of Θ at 3,854 m, with a range of about 0.04°C, can be used to indicate the variations of the LCPW and also L-PMOC. The potential temperature decreased to about 1.20°C in December 2016, and this value was maintained until June 2017, indicating an intrusion of LCPW below 3,854 m during this period. The potential temperature started increasing in July, reaching to about 1.23°C by September and then decreasing to 1.21°C by November. In the lower deep layer with Θ less than 1.2°C, the relatively low (high) Θ corresponds to the intensified northward (weak oscillation) flow (Figure 2h). The negative correlation between Θ and the meridional velocity was also found in the previous record of 1997 at 3,720 and 4,220 m (Siedler et al., 2004). For the recent record at 3,290 m, the average potential temperature of 1.32°C is close to but still above the lower boundary of UCPW. However, the seasonal

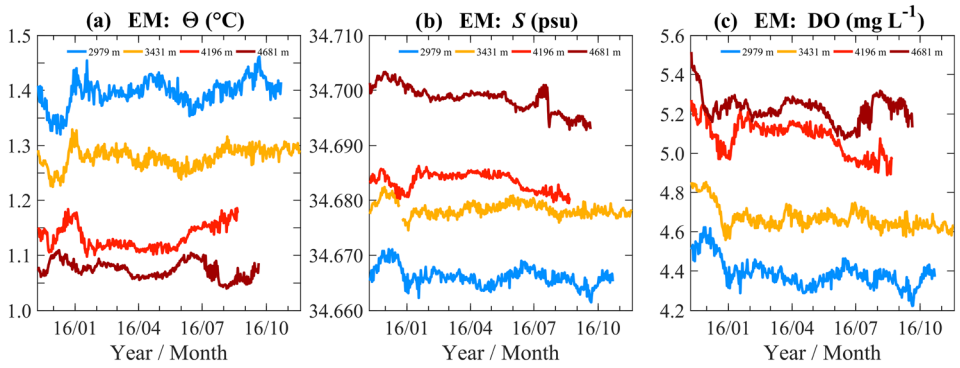

Figure 6. Time series of observed daily (a) potential temperature (Θ), (b) salinity (*S*), and (c) dissolved oxygen (DO) from 9 November 2015 to 17 November 2016. All data are from the EM observation.

phases of Θ and *S* at 3,290 m are opposite to those at 3,854 m. The value of Θ at 3,209 m was relatively high near 1.34°C from December 2016 to May 2017 and then decreased to a low value of ~1.31°C from June to November 2017. In the upper deep layer with Θ in the range of 1.2–2.2°C, a decrease in Θ corresponded to a decrease in northward flow (Figure 2f), making the correlation between Θ and deep flow positive.

Observations on the eastern side of the YMJ channel generally show consistent variations of watermass properties with that at the WM site. The annual harmonic of Θ at 2,973 and 4,162 m and *S* at 2,973 m generally explains more than 66% of the variance of 91-day running mean observations. When the phase shifts from December–May to June–November during 2016–2017, the watermass became cooler and warmer at 2,973 and 4,162 m, respectively (Figures 5c and 5d). At 2,973 m, the time-averaged Θ and *S* values are 1.40°C and 34.671 psu, and the relatively low Θ during June–November corresponds to the appearance of large southward flow at 3,009 m (Figure 4a), suggesting that this southward flow is U-PMOC. At 4,162 m, the time-averaged Θ and *S* values are 1.15°C and 34.688 psu, and the relatively low Θ during December–May appears to correspond to southward return flow of L-PMOC at 4,120 m (Figure 4c).

During the period of 9 November 2015 to 17 November 2016, observations of Θ, *S*, and the concentration of DO at the EM site are also available (Figures 6a–6c). Records at the four deep depths of 2,979, 3,431, 4,196, and 4,681 m show that decreasing Θ generally corresponds to increasing *S* and DO. The depth of 4,196 m is close to but still below the depth of the upper boundary of the LCPW, as suggested by the time-averaged Θ and *S* values of 1.13°C and 34.683 psu, respectively. During February–May 2016, the watermass is characterized by low Θ and high *S* and DO at 4,196 m. From June to September (when the record was terminated at this depth due to battery failure), Θ increased while *S* and DO decreased. Interestingly during July 2016, the watermass properties at 4,196 m and 4,681 m show opposite trends: The decreasing Θ and increasing *S* and DO at 4,681 m may indicate the rising in height of the Antarctic Bottom Water below (Johnson, 2008), hence the thinning of the LCPW layer. The depth of 2,979 m is shallower than the depth of the lower boundary of the UCPW, and the variations of its watermass properties may be strongly influenced by the upper ocean eddy and topographic Rossby waves (Ma et al., 2019) at intraseasonal timescale. This may account for the fact that the change of watermass properties at 2,979 m from December–May to June–November is not as pronounced as that at 2,973 m during 2016–2017 (Figures 5c and 5d).

A CTD/LADCP section with nine stations was made across the YMJ channel during the mooring maintenance period on 21–22 November 2016 (Figure 7). This provides an opportunity to examine the snapshot of watermass distribution and deep current transport across the whole channel. At this time, the LCPW intrusion and associated northward flow were present on the western side of the channel (Station S6), consistent with the scenario during December–May. Prior to estimating the volume transport through the observed section, two interpolations were applied to four LADCP meridional velocity (*V*) profiles (S3–S6 stations) within the channel following the method of Sprintall et al. (2012). First, we assign the deepest measured velocity to the missing data below (i.e., a slab model). Second, we assume zero velocity in the last kilometer bin nearest the sidewalls and assign the measured *V* at Stations S6 and S3 to the missing data westward and eastward, respectively. The volume transport of the L-PMOC for Θ less than 1.2°C across the observed

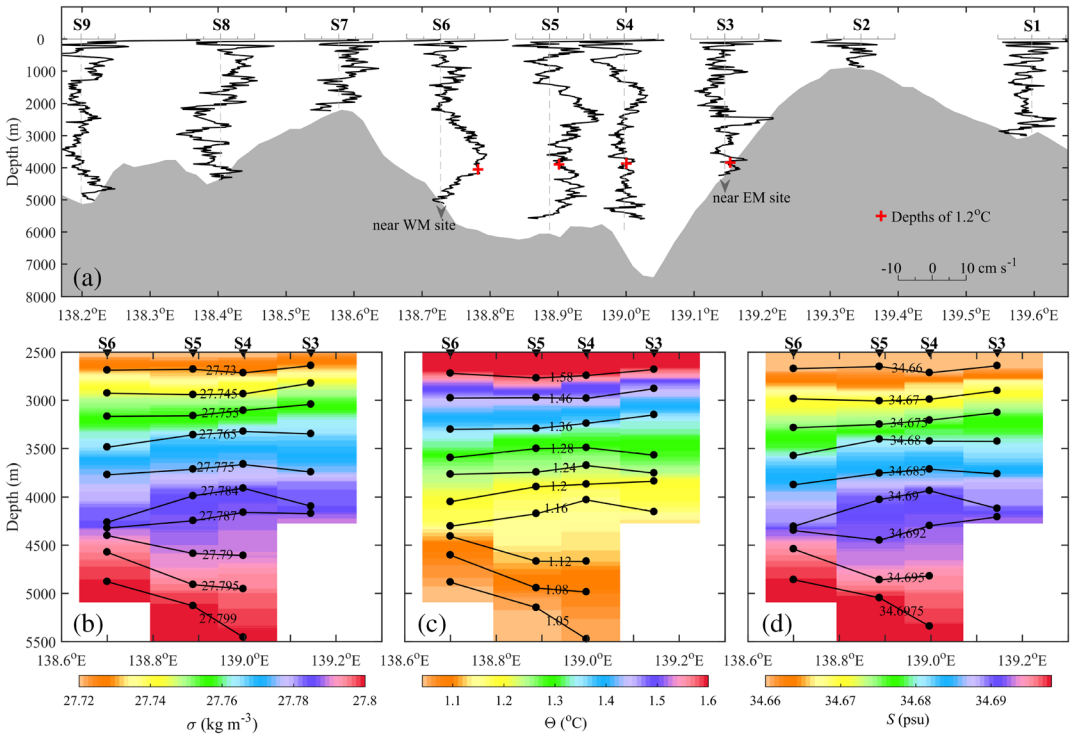

Figure 7. Longitude-depth section of (a) meridional velocity observed by LADCP and (b) potential density (σ), (c) potential temperature (Θ), and (d) salinity (S) observed by CTD along 11.35°N across the YMJ channel from 21 to 22 November 2016. The station names are marked at the top of each subplot. In panel a, red plus sign denotes the depth of Θ = 1.2°C, and bathymetry (gray shading) is obtained from Seabeam multibeam echo sounding data. In panels b–d, only profiles of four stations within the channel are shown.

section is 2.2 Sv (1 Sv = 10^6 m^3 s^{-1}), suggesting the northward net transport of LCPW during this measurement time.

The deep flow in the YMJ channel could be influenced by the presence of strong upper ocean eddies. For example, from December 1996 to January 1997, two cyclonic eddies passed near the WM96 site (Figures 8a and 8b). In order to quantify the time variations of the eddy intensity, we compute the daily time series of $SLA_m \times SLA_{std}$ over a box of 3° × 3° in longitude/latitude centered at the WM96 site (Figure 8c). Here, SLA_m and SLA_{std} are the spatial mean and the standard deviation of SLAs over the box at each day. When a strong anticyclonic (cyclonic) eddy passes by the mooring site, SLA_m has large positive (negative) values, and SLA_{std} has large positive values. During the periods when the two eddies passed near the moorings, the eddy intensity reached a peak value of ~ −0.018 m^2 (Figure 8c), and the correlation between AVISO surface geostrophic current and the observed deep flow in the meridional direction was generally higher than 0.50 (red curves in Figure 3). This suggests that these two energetic eddies could enhance the northward deep flow.

To summarize this section, recent mooring observations in the YMJ channel are analyzed and compared with a record from the late 1990s. The following characteristics are revealed. (i) The deep currents at the YMJ exhibit seasonal variation. On the western side, the strong northward flow below ~3,800 m can persist from December to May, followed by the weak flow lasting from June to November. On the eastern side, the southward flow at 5,068 m, in the lower portion of deep layer, follows the same seasonal phase as the northward flow on the western side. The southward flow within shallower deep layers (3,009 and 3,798 m) also has seasonal variation, especially during 2016–2017, but their phases are opposite to that at 5,068 m. (ii) During December–May, the deep currents at the YMJ are dominated by northward L-PMOC in the lower deep layer on the western side, which is accompanied by a relatively weak return southward flow in the lower deep layer on the eastern side. This suggests that the net volume transport of LCPW in the YMJ channel is still northward during December–May. In support of this point, the observations along a CTD/LADCP

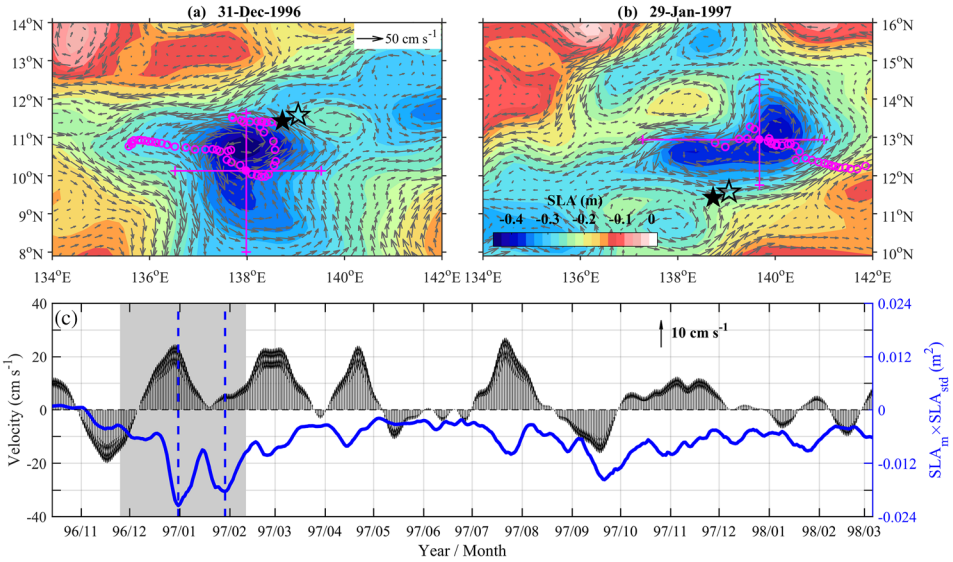

Figure 8. Maps of altimeter SLA (shading, in m), surface geostrophic velocities (arrows), and eddy edge (crosses) on (a) 31 December 1996 and (b) 29 January 1997 when two energetic cyclonic eddies strongly influenced the deep flow. In panels a and b, magenta circles denote central tracks of eddies, and solid and blank black pentagrams denote locations of the moorings WM and EM. (c) Stick plots of meridional component of AVISO surface geostrophic current at the WM site from 14 October 1996 to 6 March 1998. In panel c, blue curve shows the product of the spatial mean and standard deviation of SLA ($SLA_m \times SLA_{std}$), calculated over a box of 3° × 3° in longitude/latitude centered at the WM96 site. Two blue dashed lines indicate the dates of two cyclonic eddies shown in panels a and b. Gray shading denotes the period when upper ocean eddies exerted influence on deep flow.

section across the YMJ channel provides an estimated net northward LCPW transport of 2.2 Sv. (iii) During June–November, the deep currents at the YMJ are dominated by the southward U-PMOC in the upper deep layer on the eastern side. The deep currents on the western side and in the lower deep layer of the eastern side become very weak. (iv) Variations of the deep flow correspond to changes in the watermass properties, with the presences (absences) of northward L-PMOC and its return flow in the lower deep layer and southward U-PMOC in the upper deep layer being accompanied by lower (higher) temperature and higher (lower) salinity and dissolved oxygen concertation. (v) Energetic upper ocean eddies could influence the variations of the L-PMOC.

4. Dynamics of Seasonal Variation

In order to explore the dynamics underlying the complicated seasonal and spatial variations of deep flow in the YMJ channel revealed by observations, the MO model outputs are analyzed in this section. To assess the ability of MO to simulate observed seasonal variations of deep currents on the western and eastern sides of the channel, we evaluatethe correlation coefficients (r) and the root-mean-square deviation ($RMSD = \sqrt{\frac{1}{n}\sum_{1}^{n}(V_{observation} - V_{MO})^2}$, where n is the number of data values) between the observed records and the MO outputs of the daily time series of 91-day running mean meridional velocity. We also examine the seasonal cycle of the MO meridional velocity during 2013–2018 by applying a 91-day running mean and then an annual harmonic fit and computing the explained variance (R^2, Figure 9). The MO outputs reproduce the observed deep flows at 4,405 m of WM and at 3,009 and 3,798 m of EM quite well. In these three layers, r exceeds 0.61, RMSD is less than 2.6 cm s^{-1}, and R^2 for seasonal cycle in the MO is greater than 58% (Figures 9c–9e). For two shallower depths (3,325 m and 3,888 m) at the WM site, the MO results show a significant seasonal cycle with R^2 greater than 66%, and good performance in reproducing the observed seasonal variations of currents with high r larger than 0.67, respectively, but have biases in the time-mean velocity with large RMSD (Figures 9a and 9b). For the deeper layers (4,210 and 5,068 m) of EM, the MO results show a poor performance because the modeled deep flows have opposite direction but similar seasonal phase compared to observations, leading to negative correlation

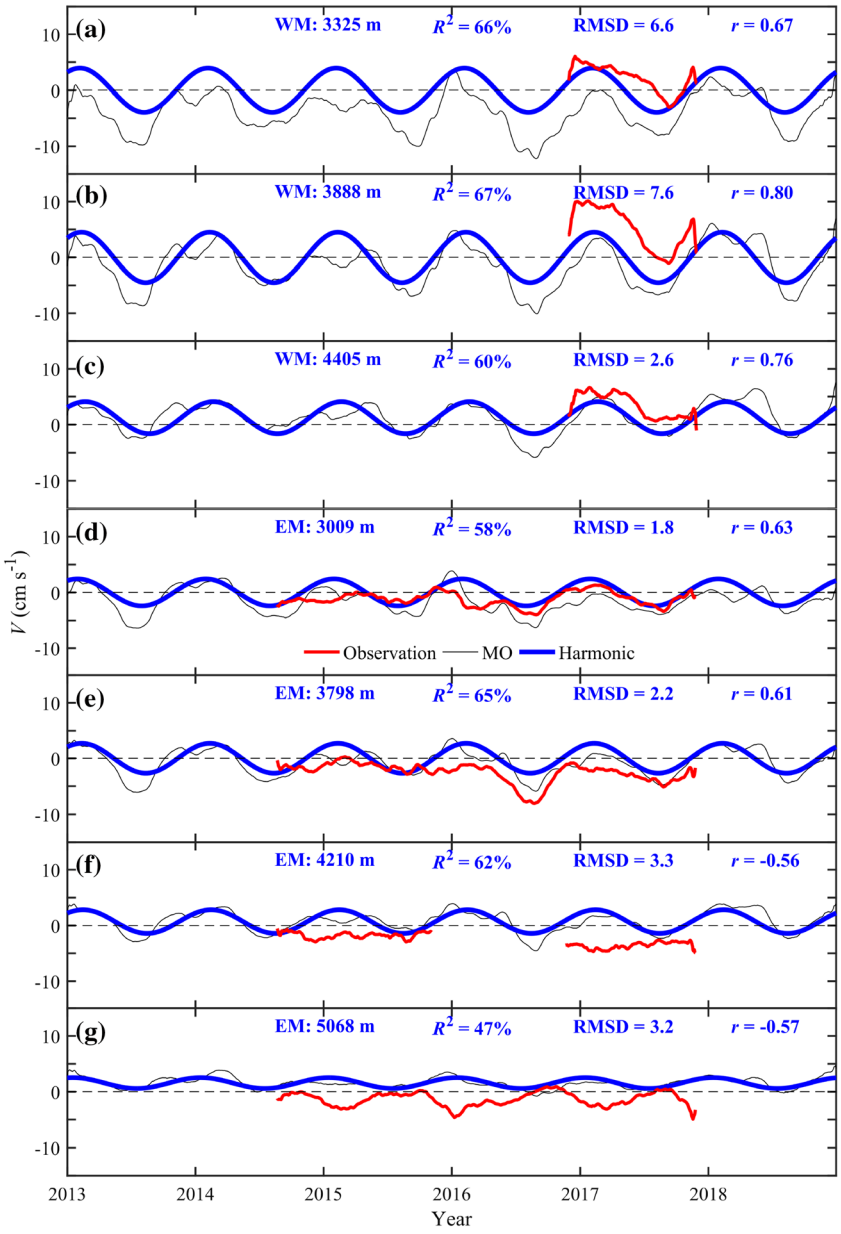

Figure 9. Time series of 91-day running-mean observed (red) and modeled (black) deep meridional velocities at the (a–c) WM and (d–g) EM sites. The annual harmonic of modeled meridional velocities (blue) are superimposed. The mean depths of the records, root-mean-square errors (RMSE) of MO relative to observation, correlation coefficients (r) between MO and observation, and explained variances (R^2) for the annual harmonic of modeled meridional velocities during 2013–2018 are denoted in each panel.

(Figures 9f and 9g). The MO results perform well at depths greater than 4,200 m at the WM site and shallower than 4,000 m at the EM site, where the intrusions of the northward L-PMOC and southward U-PMOC mainly occur.

Using the MO outputs, the composites of potential density, potential temperature, salinity, and meridional velocity during two different periods are constructed. Figure 10 shows the longitude-depth variations of these variables averaged over 11.3–11.6°N and over December–May and June–November. First, for the June–November period, the reference level of no motion for the geostrophic flow is assumed to lie deeper than ~4,500 m for both the WM and EM sites based on the observed velocities (Figure 9), this being consistent with the absence of the LCPW intrusion. According to the thermal wind relationship, isopycnals over

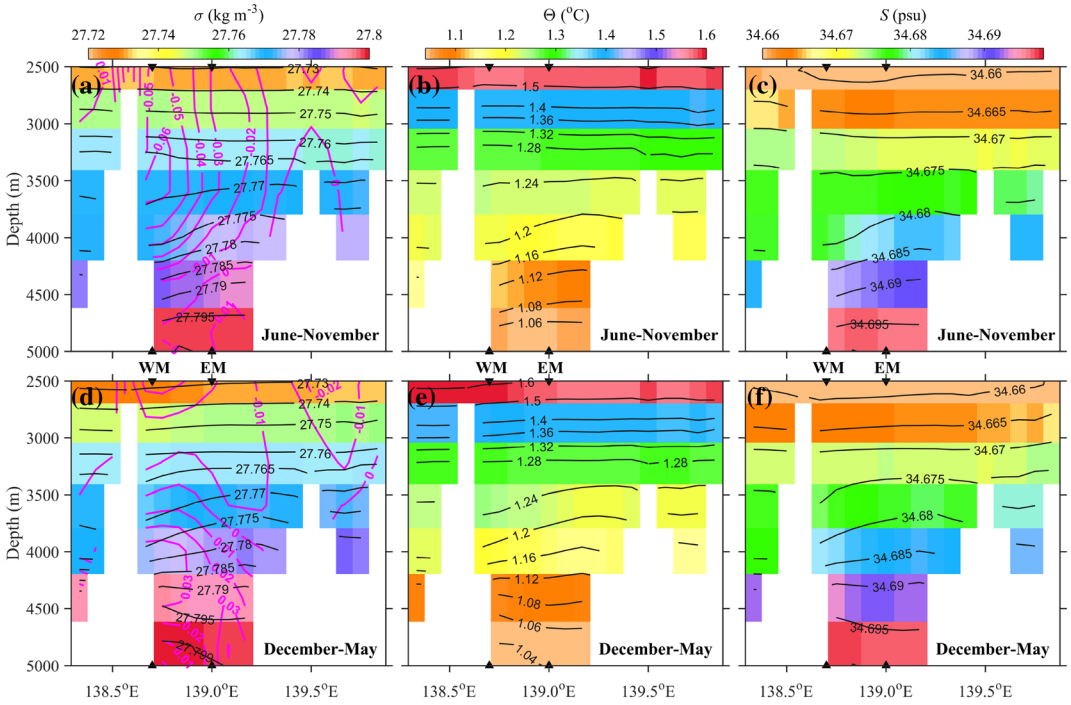

Figure 10. Composite longitude-depth section of MO modeled potential density (σ, left), potential temperature (Θ, middle), and salinity (S, right) averaged over 11.3–11.6°N during periods over (a–c) June–November and (d–f) December–May. In panels a and d, the corresponding MO meridional velocities (magenta contours) are superimposed. The mooring sites (WM and EM) are marked at the top and bottom of each subplot.

3,500–4,500 m and above 3,500 m should be inclined upward and downward from west to east (same hereinafter) on the eastern side of the channel, corresponding to an increase and then decrease in southward flow at the EM site. This puts the maximum geostrophic southward flow speed at ~3,500 m. The deep flow at the WM site was weak with a north-south-oriented oscillation, suggesting that the isopycnals on the western side may be close to horizontal on average. Therefore, the isopycnals below 3,500 m are generally slanted upward, suggesting higher density (low temperature and high salinity) at each depth on the eastern side of the channel (Figures 10a–10c). This is consistent with the observation that the density at 4,162 m of EM is generally higher than that at 4,363 m of WM during June–November (Figure 11e).

The reason for upward sloping isopycnals below 3,500 m during June–November can be explained by examining the horizontal distribution of density over a larger area. The GDEM climatology reproduces the upward sloping isopycnals in this channel quite well. Figure 11d shows the GDEM climatological density, and it can be seen that at 3,800, 4,000, and 4,200 m depths, the GDEM climatology shows that the potential density decreases from southeast to northwest (Figures 11a–11c). For the localized region around the YMJ, the exchange of watermass between the East and West Mariana Basins below 4,000 m can only occur through the deep channel, where our moorings were deployed (labeled as Channel A in Figure 11a). At shallower depth of 3,800 m, the two basins can also be connected through another deep channel (labeled as Channel B in Figure 11a), located northeast of Channel A. Furthermore, given that the density over 3,800–4,000 m in Channel B is higher than that in Channel A, we deduce the watermass transport at 3,800 m in Channel B to be larger than that in Channel A. This is consistent with the upward sloping isopycnals in Channel A during June–November. Note that the monthly field of the GDEM climatology below 3,000 m does not show seasonal variations (figure not shown) and thus cannot be used to study the situation during December–May.

Next, we discuss the period of December–May. The reference levels of no motion for the geostrophic flow should be located at ~3,000 m for the WM site and ~3,500 m for the EM site according to observed velocities (Figure 9). Based on the thermal wind relationship, isopycnals between 3,000 and 4,200 m and below

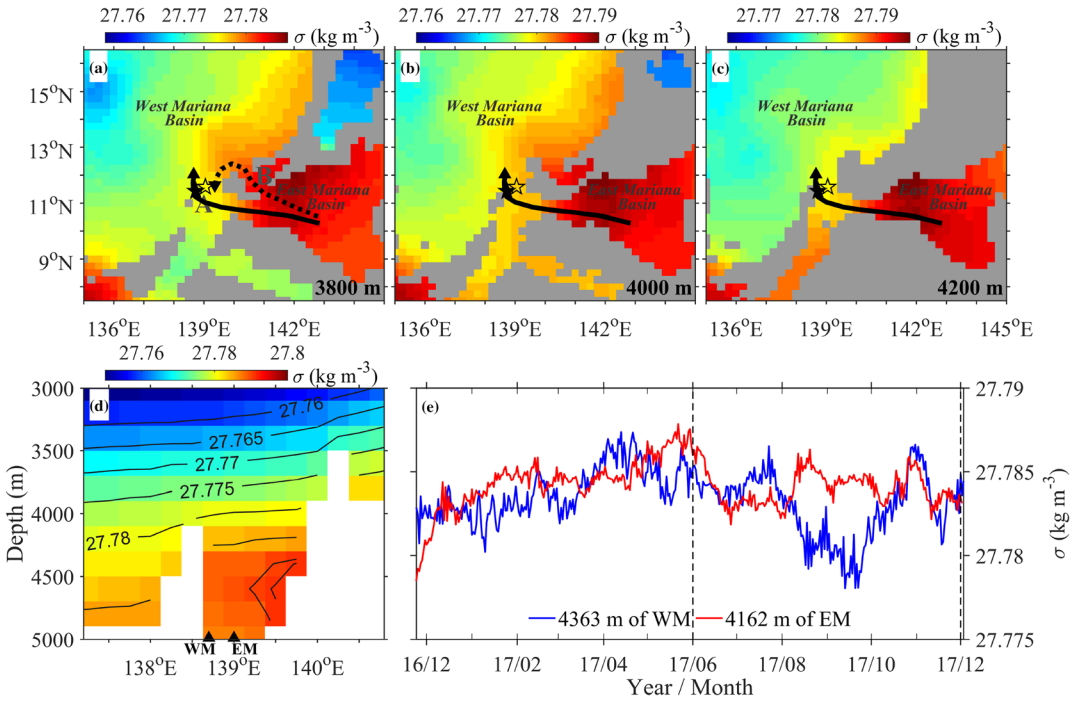

Figure 11. The horizontal distributions of GDEM climatological potential density (σ) at (a) 3,800, (b) 4,000, and (c) 4,200 m depths in the West and East Marianna Basins. The locations of the mooring sites (WM and EM, black pentagrams) and the deep channels (A and B) are marked on the maps. The schematic pathways of L-PMOC (solid arrow) and U-PMOC (dashed arrow) are superimposed. (d) Longitude-depth section of GDEM climatological potential density along 11.35°N. The mooring sites (WM and EM) are marked at the bottom. (e) Time series of observed daily potential density at 4,636 m of WM (blue) and at 4,162 m of EM (red) from 24 November 2016 to 3 December 2017. Dashed lines are used as reference lines to separate two seasonal phase.

4,200 m should be inclined upward and downward from west to east on the western side of the channel, corresponding to an increase and then decrease in northward flow. This generates the maximum northward geostrophic velocity at ~4,200 m at the WM site. A downward tilt of the isopycnals below 4,200 m is also consistent with the intrusion of the LCPW with relatively low potential temperature (Figure 10e) and high salinity (Figure 10f). This is generally consistent with the structures of the observed and modeled meridional velocities (Figures 3, 9, and 10d). However, the modeled upward sloping isopycnals over 3,000–4,200 m at the WM site may be much steeper than in reality, as the model predicts a larger decrease in northward flow as compared to observations. On the eastern side of the channel, deep flow speed in observations and the MO outputs both show an increasing trend from the level of no motion to ~4,200 m and then a decreasing trend from ~4,200 m to the bottom (~5,000 m), but the flow directions are opposite, that is, southward and northward, respectively (Figure 9). This may imply that isopycnals across the EM site should be inclined downward and then upward, opposite to the situation in the MO outputs (Figure 10d). The failure of MO outputs in reproducing the return flow on the eastern side of the channel could be due to the low horizontal resolution in this region with complicated topography. During 21–22 November 2016, a CTD survey along the section across the channel at 11.35 N indicates that the LCPW intrusion and associated northward flow were present at the WM site (Figure 7a). Thus, this section result represents the situation during the period of December–May. The observed distribution of isopycnals generally supports the above inferred scenario (Figure 7b); however, the isopycnal structure around the mooring sites cannot be determined due to insufficient longitudinal resolution of the observations.

Based on observations, model outputs, and available climatology, the dynamic interpretation for the seasonal and spatial characteristics of the deep currents in the YMJ channel can be depicted schematically (Figure 12). The following characteristics are shown. (i) The observed seasonal and spatial variations of deep currents are attributed to seasonal intrusions of both LCPW and UCPW, which in turn change the

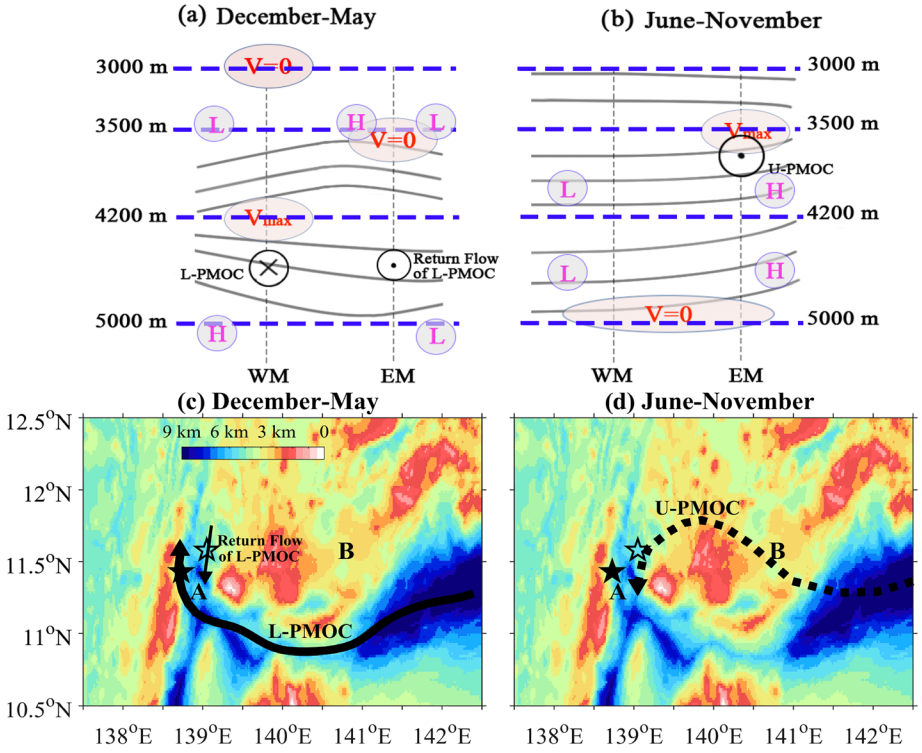

Figure 12. Schematic diagrams of characteristics of deep currents and associated isopycnals during the LCPW intrusion period over December–May (left) and during the UCPW intrusion period over June–November (right) in the YMJ channel. In panels a and b, gray lines denote the isopycnals, the capitals L and H denote the low and high density, the cross and dot symbols denote northward (L-PMOC) and southward (return flow of L-PMOC and U-PMOC) flows, and $V = 0$ and V_{max} indicate the reference level of no motion and the location of the maximum flow speed during each period. In panels c and d, bold solid, thin solid, and dashed lines depict the schematic pathways of L-PMOC, the return flow of L-PMOC, and U-PMOC, respectively. Locations of the mooring sites (WM and EM) are marked by dashed lines in panels a and b and black pentagrams in panels c and d.

distribution of isopycnal surfaces and deep currents through geostrophic balance. (ii) During June–November, the isopycnals are slanted upward with higher density in the east below 3,500 m, accompanied by an absence of the L-PMOC at the WM site and the presence of the southward U-PMOC at the EM site (Figure 12b). The upward sloping isopycnals are attributed to the inflow of high-density water from the East Mariana Basin through the deep Channel B (Figure 12d). (iii) During December–May, the isopycnals below and above ~4,200 m are changed to form downward-sloping and upward convex shapes, accompanied by the presence of the northward L-PMOC in the west and its southward return flow in the east in the lower deep layer and the absence of the southward U-PMOC in the east in the upper deep layer (Figures 12a and 12c).

5. Discussion and Conclusions

Two separate mooring observations in the 1990s and 2010s show remarkably similar seasonal variation of deep currents on the western side of the YMJ channel. Differences are also present, indicating the interdecadal variation of the PMOC. Previous studies have suggested that the L-PMOC in the Pacific undergoes changes both in strength and temperature in recent decades (Fukasawa et al., 2004; Johnson et al., 2007; Kouketsu et al., 2011; Purkey & Johnson, 2010, 2012; Voet et al., 2016). Figure 13a shows the time series of depth-integrated currents over 3,800–4,400 m on the western side of the channel in the 1990s and 2010s. The time means and standard deviations of depth-integrated current over their overlapped months (i.e., from December to next November) are 43.50 ± 43.53 m^2 s^{-1} in the 1990s and 26.78 ± 25.52 m^2 s^{-1} in 2010s. The time-mean of depth-integrated current was reduced by 38% compared to the observed value of two decades ago. This reduction of 38% is probably influenced by the two strong eddies from December 1996 to

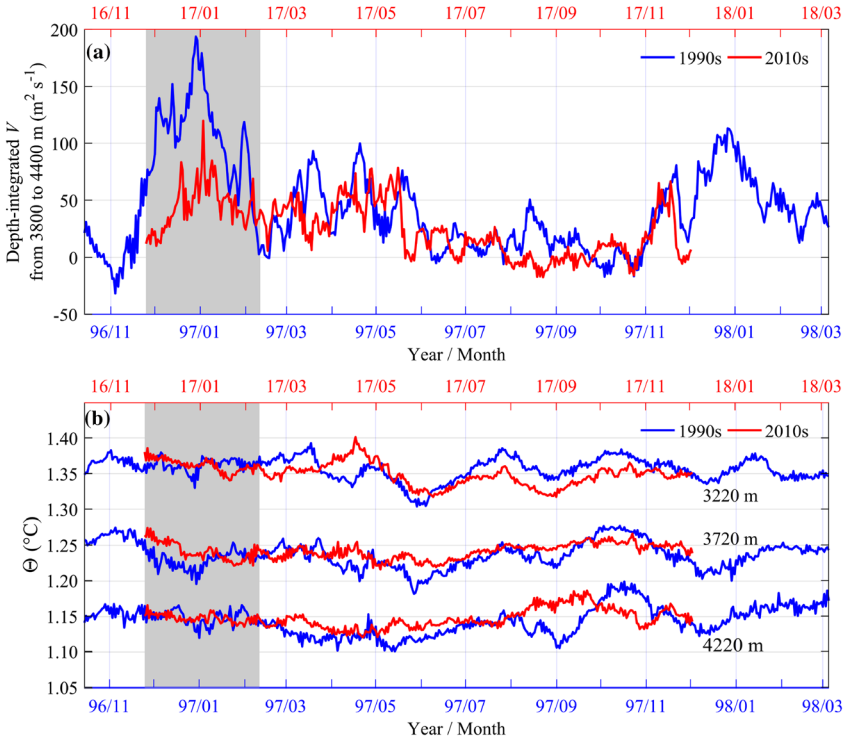

Figure 13. Time series of (a) depth-integrated meridional velocity (V) from 3,800 to 4,400 m and (b) potential temperature (Θ) at three layers at the WM site in the 1990s (blue) and 2010s (red). Potential temperature in the 1990s was derived from in situ temperature observed by current meters being adapted to CTD cast values obtained during mooring recovery. Potential temperature in the 2010s was derived from interpolation from adjacent observed layers. Gray shadings in panels a and b denote the periods when upper ocean eddies exerted influence on deep flow.

January 1997 (gray shaded period), which enhanced the northward velocity. If we exclude the period of eddy influence, the time means and standard deviations of depth-integrated current are 26.88 ± 25.47 m^2 s^{-1} in 1990s and 21.48 ± 23.74 m^2 s^{-1} in 2010s, and the reduction becomes 20%, which is slightly smaller but generally comparable to 27% on the western side of the Samoan Passage (Voet et al., 2016). However, in terms of uncertainty caused by the limited length of the time series (Voet et al., 2016), this reduction is only statistically significant at the 68% confidence level (± 3.5 m^2 s^{-1}) and not within the 95% confidence level (± 7.1 m^2 s^{-1}). Nevertheless, the reduction in deep currents at the YMJ agrees with several studies that suggested a slowdown of the PMOC in recent decades (Kouketsu et al., 2011; Voet et al., 2016). We further compare the time-mean temperatures of the deep flow in the 1990s and 2010s (Figure 13b). During their overlapped months excluding the strong eddy period, the time means and standard deviations of potential temperatures at 3,220, 3,720, and 4,220 m are 1.356 ± 0.018°C, 1.236 ± 0.020°C, and 1.138 ± 0.022°C in 1990s and 1.347 ± 0.016°C, 1.241 ± 0.011°C, and 1.147 ± 0.015°C in 2010s. The time-mean temperature becomes slightly colder (−0.009°C) at 3,220 m and slightly warmer (0.005°C and 0.009°C) at two deeper layers. However, their variations over 20 years are within the accuracy of RCM8 temperature sensors (± 0.03°C) that were used in the 1990s and thus statistically not different from zero. We may speculate that there has been no significant warming in the deep ocean of the western Pacific since 1990s. This agrees with the previous study of Purkey and Johnson (2010) suggesting very weak heat flux across 4,000 m in the North Pacific.

In conclusion, this study first reveals the seasonal variability of the L-PMOC and U-PMOC in the YMJ channel based on two mooring observations made 20 years ago and recently, which is closely associated with the seasonal LCPW and UCPW intrusions. The variability of deep current and watermass properties is closely linked through geostrophic balance. The cross-channel Rossby number is estimated according to $R_L = \frac{l^2 V}{L^2 f l}$, where $l \approx 80$ km and $L \geq 200$ km are the width scales in the cross- and along-channel

directions, respectively; $V \approx 10$ cm s^{-1} is the along-channel velocity scale, and $f = 3 \times 10^{-5}$ s^{-1} is Coriolis parameter. The estimated R_L is less than $O(0.1)$, consistent with the establishment of a geostrophic balance in the cross-section of this channel (Chong et al., 2000; Overland, 1984). During June–November, the deep currents were dominated by the southward U-PMOC in the upper deep layer on the eastern side of the channel. This corresponds to isopycnals that slope upward towards the east below 3,500 m in our observations, accompanied by the inflow of high-density water from East Mariana Basin through the northeastern shallower deep channel. The southward U-PMOC in the YMJ channel may flow into the West Caroline Basin through the Yap trench and finally arrive in the Philippine Basin via the deep channel near the western boundary. During December–May, the deep currents at the YMJ were dominated by the northward L-PMOC in the lower deep layer on the western side, which was accompanied by a relatively weak return southward flow also in the lower deep layer on the eastern side. Correspondingly, the isopycnals below and above ~4,200 m are likely changed to form downward-sloping and upward convex shapes from west to east. In addition, energetic upper ocean eddies could influence the variations of the PMOC below 3,800 m.

The mechanism for the seasonal LCPW and UCPW intrusions into the YMJ channel may be related to the pressure gradient force between two adjacent basins but is not investigated in this study. The pressure gradient can be formed regionally or globally through a number of physical processes, such as the deep ocean mixing (Zhou et al., 2014), the route shift of deep inflows (Huang et al., 2018), or seasonal watermass formation at high latitudes. The seasonal formation of bottom water near the Antarctic shelf has been documented (e.g., Evans et al., 2014; Fukamachi et al., 2000; Koshlyakov & Tarakanov, 2003; Williams et al., 2008) and may factor in the YMJ channel since the PMOC is supplied only from the south. Furthermore, seasonal changes in watermass area of LCPW and UCPW near the Antarctic shelf show different phases. In austral summer (winter), the area of UCPW and LCPW increases (decreases) and decreases (increases), respectively (Evans et al., 2014). This may be related to the opposite seasonal phase of U-PMOC and L-PMOC in the YMJ channel. The link of the seasonality between the YMJ and its upstream regions needs to be further explored. Ultimately, this will contribute to the more comprehensive understanding of the structure, variability, and climate effect of the PMOC.

Data Availability Statement

Mooring data analyzed in this paper are available for download online (https://doi.org/10.5281/zenodo.3755279). Mercator Ocean model outputs are obtained from Copernicus Marine Environment Monitoring Service (http://marine.copernicus.eu/). AVISO data are also obtained from the above website.

Acknowledgments

We thank Drs. Gerold Siedler, Walter Zenk, and Thomas J. Müller for providing their mooring and CTD profile data. The crew of R/V Kexue (Science) is thanked for their assistance with the deployment and retrieval of the moorings. This study is supported by the National Natural Science Foundation of China (grants 91958204 and 41776022), the Strategic Priority Research Program of the Chinese Academy of Sciences (grant XDA22000000), the Key Research Program of Frontier Sciences, CAS (grant QYZDB-SSW-SYS034). F. Wang thanks the support from the Scientific and Technological Innovation Project by Qingdao National Laboratory for Marine Science and Technology (grant 2016ASKJ12), the National Program on Global Change and Air-Sea Interaction (grant GASI-IPOVAI-01-01), and the National Natural Science Foundation of China (grants 41730534 and 41421005). L. Pratt gratefully acknowledges the support by NSF (grant OCE-1657870). Jianing Wang and Qiang Ma contributed equally to this work.

References

Callahan, J. E. (1972). The structure and circulation of deep water in the Antarctic. *Deep Sea Research*, *19*, 563–575.

Carnes, M. R. (2009). Description and evaluation of GDEM-V 3.0, NRL Rep. *NRL/MR/7330-09-9165*, Nav. Res. Lab., Washington, D. C.

Chaigneau, A., Gizolme, A., & Grados, C. (2008). Mesoscale eddies off Peru in altimeter records: Identification algorithms and eddy spatio-temporal patterns. *Progress in Oceanography*, *79*(2–4), 106–119. https://doi.org/10.1016/j.pocean.2008.10.013

Chong, J. C., Sprintall, J., Hautala, S., Morawitz, W. L., Bray, N. A., & Pandoe, W. (2000). Shallow throughflow variability in the outflow straits of Indonesia. *Geophysical Research Letters*, *27*(1), 125–128. https://doi.org/10.1029/1999GL002338

Evans, D. G., Zika, J. D., Naveira Garabato, A. C., & Nurser, A. G. (2014). The imprint of Southern Ocean overturning on seasonal water mass variability in Drake Passage. *Journal of Geophysical Research: Oceans*, *119*, 7987–8010. https://doi.org/10.1002/2014JC010097

Fukamachi, Y., Wakatsuchi, M., Taira, K., Kitagawa, S., Ushio, S., Takahashi, A., et al. (2000). Seasonal variability of bottom water properties off Adélie Land, Antarctica. *Journal of Geophysical Research*, *105*(C3), 6531–6540. https://doi.org/10.1029/1999JC900292

Fukasawa, M., Freeland, H., Perkin, R., Watanabe, T., Uchida, H., & Nishina, A. (2004). Bottom water warming in the North Pacific Ocean. *Nature*, *427*(6977), 825–827. https://doi.org/10.1038/nature02337

Huang, C., Xie, Q., Wang, D., Shu, Y., Xu, H., Xiao, J., et al. (2018). Seasonal variability of water characteristics in the challenger deep observed by four cruises. *Scientific Reports*, *8*(1), 11791. https://doi.org/10.1038/s41598-018-30176-4

Johnson, G. C. (2008). Quantifying Antarctic bottom water and North Atlantic deep water volumes. *Journal of Geophysical Research*, *113*, C05027. https://doi.org/10.1029/2007JC004477

Johnson, G. C., Mecking, S., Sloyan, B. M., & Wijffels, S. E. (2007). Recent bottom water warming in the Pacific Ocean. *Journal of Climate*, *20*(21), 5365–5375. https://doi.org/10.1175/2007JCLI1879.1

Johnson, G. C., Rudnick, D. L., & Taft, B. A. (1994). Bottom water variability in the Samoa passage. *Journal of Marine Research*, *52*(2), 177–196. https://doi.org/10.1357/0022240943077118

Johnson, G. C., & Toole, J. M. (1993). Flow of deep and bottom waters in the Pacific at 10 N. *Deep Sea Research Part I: Oceanographic Research Papers*, *40*(2), 371–394. https://doi.org/10.1016/0967-0637(93)90009-R

Kawabe, M., & Fujio, S. (2010). Pacific Ocean circulation based on observation. *Journal of Oceanography*, *66*(3), 389–403. https://doi.org/10.1007/s10872-010-0034-8

Kawabe, M., Fujio, S., & Yanagimoto, D. (2003). Deep-water circulation at low latitudes in the western North Pacific. *Deep Sea Research Part I: Oceanographic Research Papers*, *50*(5), 631–656. https://doi.org/10.1016/S0967-0637(03)00040-2

Kawabe, M., Fujio, S., Yanagimoto, D., & Tanaka, K. (2009). Water masses and currents of deep circulation southwest of the Shatsky rise in the western North Pacific. *Deep Sea Research Part I: Oceanographic Research Papers*, *56*(10), 1675–1687. https://doi.org/10.1016/j.dsr.2009.06.003

Kawabe, M., Yanagimoto, D., & Kitagawa, S. (2006). Variations of deep western boundary currents in the Melanesian Basin in the western North Pacific. *Deep Sea Research Part I: Oceanographic Research Papers*, *53*(6), 942–959. https://doi.org/10.1016/j.dsr.2006.03.003

Koshlyakov, M. N., & Tarakanov, R. Y. (2003). Antarctic circumpolar water in the southern part of the Pacific Ocean. *Oceanology*, *43*(5), 607–621. https://doi.org/10.1016/S0399-1784(03)00036-7

Kouketsu, S., Doi, T., Kawano, T., Masuda, S., Sugiura, N., Sasaki, Y., et al. (2011). Deep ocean heat content changes estimated from observation and reanalysis product and their influence on sea level change. *Journal of Geophysical Research*, *116*, C03012. https://doi.org/10.1029/2010JC006464

Lellouche, J. M., Greiner, E., Galloudec, O. L., Garric, G., Regnier, C., Drevillon, M., et al. (2018). Recent updates to the Copernicus marine service global ocean monitoring and forecasting real-time 1/12° high-resolution system. *Ocean Science*, *14*(5), 1093–1126. https://doi.org/10.5194/os-14-1093-2018

Lellouche, J. M., Le Galloudec, O., Drévillon, M., Régnier, C., Greiner, E., Garric, G., et al. (2013). Evaluation of global monitoring and forecasting systems at Mercator Ocean. *Ocean Science*, *9*(1), 57–81. https://doi.org/10.5194/os-9-57-2013

Ma, Q., Wang, F., Wang, J., & Lyu, Y. (2019). Intensified deep ocean variability induced by topographic Rossby waves at the Pacific yap-Mariana junction. *Journal of Geophysical Research: Oceans*, *124*, 8360–8374. https://doi.org/10.1029/2019JC015490

Mantyla, A. W., & Reid, J. L. (1983). Abyssal characteristics of the World Ocean waters. *Deep Sea Research*, *30*(8), 805–833. https://doi.org/10.1016/0198-0149(83)90002-X

Overland, J. E. (1984). Scale analysis of marine winds in straits and along mountainous coasts. *Monthly Weather Review*, *112*(12), 2530–2534. https://doi.org/10.1175/1520-0493(1984)112<2530:SAOMWI>2.0.CO;2

Pratt, L. J., Voet, G., Pacini, A., Tan, S., Alford, M. H., Carter, G. S., et al. (2019). Pacific abyssal transport and mixing: Through the Samoan passage versus around the Manihiki plateau. *Journal of Physical Oceanography*, *49*(6), 1577–1592. https://doi.org/10.1175/JPO-D-18-0124.1

Purkey, S. G., & Johnson, G. C. (2010). Warming of global abyssal and deep Southern Ocean waters between the 1990s and 2000s: Contributions to global heat and sea level rise budgets. *Journal of Climate*, *23*(23), 6336–6351. https://doi.org/10.1175/2010JCLI3682.1

Purkey, S. G., & Johnson, G. C. (2012). Global contraction of Antarctic Bottom Water between the 1980s and 2000s. *Journal of Climate*, *25*(17), 5830–5844. https://doi.org/10.1175/JCLI-D-11-00612.1

Reid, J. L. (1997). On the total geostrophic circulation of the Pacific Ocean: Flow patterns, tracers, and transports. *Progress in Oceanography*, *39*(4), 263–352. https://doi.org/10.1016/S0079-6611(97)00012-8

Rudnick, D. L. (1997). Direct velocity measurements in the Samoan Passage. *Journal of Geophysical Research*, *102*(C2), 3293–3302. https://doi.org/10.1029/96JC03286

Siedler, G., Holfort, J., Zenk, W., Müller, T. J., & Csernok, T. (2004). Deep-water flow in the Mariana and Caroline basins. *Journal of Physical Oceanography*, *34*(3), 566–581. https://doi.org/10.1175/2511.1

Sprintall, J., Gordon, A. L., Flament, P., & Villanoy, C. L. (2012). Observations of exchange between the South China Sea and the Sulu Sea. *Journal of Geophysical Research*, *117*, C05036. https://doi.org/10.1029/2011JC007610

Visbeck, M. (2002). Deep velocity profiling using lowered acoustic Doppler current profilers: Bottom track and inverse solutions. *Journal of Atmospheric and Oceanic Technology*, *19*(5), 794–807. https://doi.org/10.1175/1520-0426(2002)019<0794:DVPULA>2.0.CO;2

Voet, G., Alford, M. H., Girton, J. B., Carter, G. S., Mickett, J. B., & Klymak, J. M. (2016). Warming and weakening of the abyssal flow through Samoan passage. *Journal of Physical Oceanography*, *46*(8), 2389–2401. https://doi.org/10.1175/JPO-D-16-0063.1

Voet, G., Girton, J. B., Alford, M. H., Carter, G. S., Klymak, J. M., & Mickett, J. B. (2015). Pathways, volume transport, and mixing of abyssal water in the samoan passage. *Journal of Physical Oceanography*, *45*(2), 562–588. https://doi.org/10.1175/JPO-D-14-0096.1

Wang, G., Xie, S. P., Qu, T., & Huang, R. X. (2011). Deep South China Sea circulation. *Geophysical Research Letters*, *38*, L05601. https://doi.org/10.1029/2010GL046626

Whitworth, T. III, Warren, B. A., Nowlin, W. D. Jr., Rutz, S. B., Pillsbury, R. D., & Moore, M. I. (1999). On the deep western-boundary current in the Southwest Pacific Basin. *Progress in Oceanography*, *43*(1), 1–54. https://doi.org/10.1016/S0079-6611(99)00005-1

Williams, G. D., Bindoff, N. L., Marsland, S. J., & Rintoul, S. R. (2008). Formation and export of dense shelf water from the Adélie depression, East Antarctica. *Journal of Geophysical Research*, *113*, C04039. https://doi.org/10.1029/2007JC004346

Zhou, C., Zhao, W., Tian, J., Yang, Q., & Qu, T. (2014). Variability of the deep-water overflow in the Luzon Strait. *Journal of Physical Oceanography*, *44*(11), 2972–2986. https://doi.org/10.1175/JPO-D-14-0113.1